Simulating the interaction between a descending super-quadric solid object and a soap film

I. T. Davies*

Department of Mathematics, Aberystwyth University,

Aberystwyth, Ceredigion SY23 3BZ, UK

Abstract

We investigate the interaction that occurs between a light solid object and a horizontal soap film of a "bamboo" foam contained in a cylindrical tube. We vary the shape of the descending object from a sphere to a cube by changing a single shape parameter. We investigate in detail how the soap film deforms and determine the forces that the film exerts on the object, depending on the radius of the cylindrical tube, and the shape, orientation and position of the object. We show that a cubic particle in a particular orientation experiences the largest drag force, and that this orientation is also the most likely outcome of dropping a cube from an arbitrary orientation through a bamboo foam.

* itd@aber.ac.uk

I. INTRODUCTION

Liquid foams are a class of materials that are widely-used both domestically and industrially [1, 2]. They are classified as complex fluids because their response to applied stress is highly non-linear: they behave as elastic solids at low stresses, exhibit plasticity at higher stresses and have an apparent yield stress above which they flow. They are two-phase materials consisting mainly of gas, with consequently a low density but also a large surface area. As a result of these remarkable properties, aqueous foams are desirable for example in personal hygiene and food products and are also integral in industrial processes such as enhanced oil-recovery [3, 4] and froth flotation for mineral separation, paper deinking, waste water treatment and soil remediation [5–9]. The process of froth flotation in particular is driven by how the surfaces within a foam interact with solid particles and objects, and gaining a better understanding of this interaction is one of the main objectives of this work.

Foams have also been studied at the microfluidic scale [10–12] where they have found new applications in medical procedures such as foam sclerotherapy for spider and varicose veins and for building new materials such as scaffolds for tissue engineering [13, 14]. In this work, we consider how the precise structure of an ordered foam could be used to control the position and orientation of particles or small objects. This has many potential applications, for example in pharmaceuticals and medicine, where controlled transportation of particles, objects or solvents through confined geometries at the micro-scale is needed [10].

We focus our attention on the interaction that occurs between a horizontal soap film contained in a vertical cylinder and a solid object that descends through it under gravity. The soap film can be thought of as one film of a "*bamboo*" foam, a structure in which a cylindrical container is filled with a single column of bubbles of equal volume. Previously we predicted that the motion of a spherical object could be controlled by an ordered foam [15]. Here, we develop 3D Surface Evolver [16] simulations to investigate how this interaction affects the final position and orientation of a non-spherical descending object. The object that we consider is small (compared to the foam's bubbles) and light, with its size and weight chosen so that the Bond number is equal to one (see §II for more details). This corresponds roughly to particles that would be found in the process of froth flotation and those that could easily be constructed for microfluidic experiments. For this value of the Bond number, surface tension effects are not dominated by the effects of gravity, and therefore a foam

should be able to strongly influence the position and orientation of the object. This is in contrast to the work of Courbin and Stone [17] and Le Goff *et al.* [18], for example, who showed that soap films and foams can absorb energy from fast moving objects with a much larger Bond number, where gravitational and inertial effects dominate any surface tension effects. They also showed that when a spherical object falls through a soap film, small bubbles can form due to air becoming trapped on impact or during the pinch off of the soap film during detachment. Our simulations do not allow for the formation of new bubbles, and we propose that the effect that such small bubbles have on the motion of a descending object is negligible. Due to the lightness of the objects that we consider, we assume that their motion as a result of the forces exerted on them by a soap film is slow compared to how fast the soap film relaxes, so our work is confined to a quasi-static regime (see §II).

Probing a foam's response to solid objects is a standard tool that has been used to develop a better understanding of their complex behaviour. In 3D, Cantat and Pitois [19, 20] measured the forces exerted by a disordered foam on a spherical bead, and detected elastic loading and topological changes, while de Bruyn [21, 22] showed that the forces exerted by a spherical bead induce a local fluidized region in the foam. In 2D, where the response of a foam to solid objects can be easily visualized, Raufaste *et al.* [23] showed that the drag force exerted on a circular object by a flowing foam increases with the size of the object and decreases with the liquid fraction of the foam. Furthermore, it was shown by Dollet et al. [24], and in our previous work [25], that liquid foams, due to their elasticity, can be used to reorient an elliptical object so that it becomes aligned with the direction of flow. Simulations by Boulogne and Cox [26] confirmed that the forces exerted by a flowing 2D foam on solid objects are highly dependent on the shape of the object. We extend this study into how the shape of the object affects how it interacts with a foam in 3D.

We will use Surface Evolver [16] simulations to study how a soap film of a bamboo foam interacts with super-quadric objects, ranging from a sphere to a rounded cube, descending under gravity from different initial positions and orientations. We assume that the object is covered by a wetting film so that the soap film always contacts the object normal to its surface. We investigate how a bamboo foam repositions and reorients such objects, and probe in detail the forces exerted on the descending object by the foam as well as the perturbation caused to the film. Our work extends the contributions by Morris *et al.* [27–29], which probe how objects such as cubes or ellipsoids and their orientations and surface

properties affect the stability of a thin film by which they are held. There are also many related contributions in biology, as reviewed by Dasgupta *et al.* [30], that show how fluid interfaces and biological membranes interact with particles of different shapes, and we see similar perturbations of the soap film in this work.

The remainder of the paper is organised as follows: The simulation model and methodology are described in detail in section II. The results of our simulations are discussed in section III, where we vary the the radius of the cylindrical container (§III A), the shape of the descending object (§III B), its initial orientation (§III C) and its initial position above the film (§III D). This is followed by our conclusions and discussion of future work in section IV.

II. METHOD

The Surface Evolver [16] allows us to resolve bubble pressures and the geometry of thin films for foams at equilibrium under given constraints. Our simulations consists of a single soap film, initially flat and horizontal, that separates two bubbles contained in a cylindrical tube. The tube has radius r_c, height $h = 10$ (which is fixed throughout) and a vertical centre-line that coincides with the z-axis of the Cartesian coordinate system, so that the centre of the cylinder's base defines the origin.

The surface of the solid object that falls through the soap film is defined by the superquadric equation

$$(x - x_0)^\lambda + (y - y_0)^\lambda + (z - z_0)^\lambda = r_s^\lambda, \tag{1}$$

where (x_0, y_0, z_0) denotes its centre coordinates, r_s its radius, and λ is a shape parameter that satisfies $\lambda = 2n$ where $n \in \mathbb{N}^+$. When $\lambda = 2$ the object is a sphere, while increasing λ yields a cube with rounded edges and corners (and letting $\lambda \to \infty$ would yield a cube) [31, 32]. For a cube, r_s describes the minimum distance from its centre to its surface, and for convenience we shall refer to this as the radius of the cube. The solid object is initially positioned above the soap film such that they do not touch (see figure 1a).

The surface tension of the soap film is 2γ and this is set to be equal to 1 throughout this work. The actual volume of bubble k (where $k = 1, 2$) is denoted by V_k. The soap film is represented by a triangulated mesh. It is equilibrated by minimizing its surface area A,

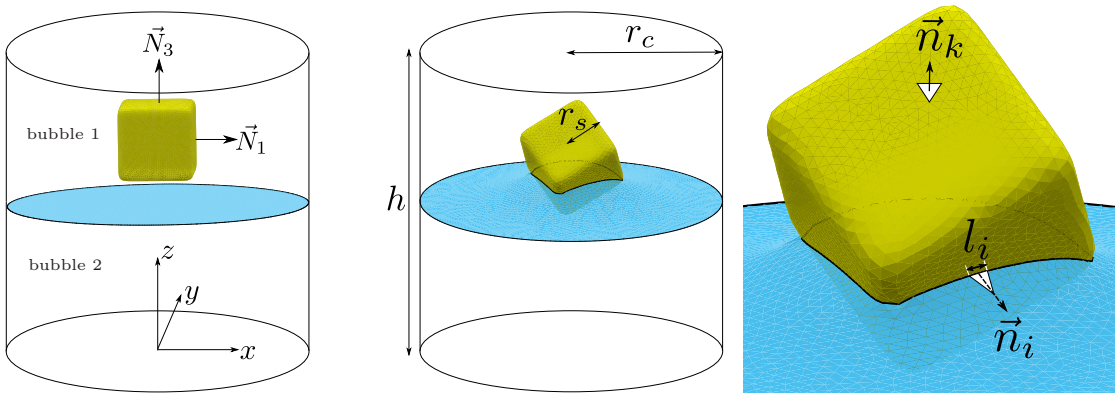

(a) (b) (c)

FIG. 1: (a) The initial set-up in which a cube is positioned above a horizontal film that separates two bubbles in a cylindrical tube with radius r_c and height h. The orientation of the cube is prescribed and then traced by recording the angle that the normal vectors that define it, $\vec{N}_1$, $\vec{N}_2$ (obscured by the cube in the image) and $\vec{N}_3$ make with the z-axis. (b) The object (of radius r_s) is allowed to fall through the soap film under gravity, and therefore deforms the soap film during contact. Its motion is governed by the resultant of its weight, mg, and the pressure and network forces that the foam exerts on it. (c) For each edge i of the triangulated surface of the soap film that contacts the object, an outward network force is exerted in the normal direction, $\vec{n}_i$ over its length l_i. Similarly, a pressure force is exerted by contacting bubbles, now in the inward normal direction to the surface, $-\vec{n}_k$, over all facets k. In the same way, bubble pressures and surface tension contribute towards a network and pressure torque which rotate the object.

using the energy functional:

$$E = 2\gamma A + \sum_k p_k \left(V_k - V_k^t\right), \tag{2}$$

where p_k is a Lagrange multiplier that denotes the pressure of bubble k. Both bubbles are assigned the same target volume,

$$V_k^t = \frac{1}{2}\left(\text{volume of cylinder - volume of solid object}\right) = \frac{1}{2}\left(2\pi r_c h - V_s\right), \tag{3}$$

where the volume of the super-quadric object is given by

$$V_s = \frac{8r_s^2}{3\lambda^2}\frac{\Gamma\left(\frac{1}{\lambda}\right)^3}{\Gamma\left(\frac{3}{\lambda}\right)}, \tag{4}$$

(as derived in [31]) and its calculation requires numerical computation of gamma functions, such as $\Gamma(a/\lambda) = \int_0^\infty t^{a/\lambda-1}e^{-t}dt$.

We set the initial orientation of the object by rotating it by prescribed angles ϕ_j, θ_j and ψ_j around the x, y and z axes respectively. This involves multiplying the surface constraint given in equation 1 by the rotation matrices

$$\mathbf{R}_{x,j} = \begin{bmatrix} 1 & 0 & 0 \\ 0 & \cos\phi_j & -\sin\phi_j \\ 0 & \sin\phi_j & \cos\phi_j \end{bmatrix}, \mathbf{R}_{y,j} = \begin{bmatrix} \cos\theta_j & 0 & \sin\theta_j \\ 0 & 1 & 0 \\ -\sin\theta_j & 0 & \cos\theta_j \end{bmatrix}, \mathbf{R}_{z,j} = \begin{bmatrix} \cos\psi_j & -\sin\psi_j & 0 \\ \sin\psi_j & \cos\psi_j & 0 \\ 0 & 0 & 1 \end{bmatrix}, \quad (5)$$

in this order, equivalent to applying the combined rotation matrix

$$\mathbf{R}_j = \mathbf{R}_{z,j}\mathbf{R}_{y,j}\mathbf{R}_{x,j}, \quad (6)$$

where the index j represents the current time step.

The object is assigned a weight, mg, chosen so that the Bond number $Bo = mgr_s^2/2\gamma V_s$ is equal to one. We fix the volume of the object at $V_s = \frac{4}{3}\pi$, that is the volume of a sphere with radius $r_s = 1$. Thus when the shape parameter λ is increased, the value of r_s is decreased (to keep the volume of the object fixed), and its weight is increased (to keep the Bond number fixed). The object is allowed to descend through the soap film under gravity. We assume that the motion of the object when in contact with the soap film is slow and overdamped so that inertial effects can be neglected. Thus we use a quasi-static model as described in previous work [15]. This model is only appropriate when the object is in contact with the soap film, which is the focus of this work. The object is lowered, and once its surface begins to overlap the soap film, the nearest facets of the soap film and the object are merged and the soap film is equilibrated using a combination of gradient descent and conjugate gradient energy minimization steps. The minimization procedure continues until convergence of E to within a tolerance of 1×10^{-5} has been achieved.

The contacting soap film exerts a network force, $\vec{F}^n$ on the solid object due to the pull of surface tension. This force is calculated geometrically as

$$\vec{F}^n = 2\gamma \sum_i l_i \vec{n}_i, \quad (7)$$

where l_i denotes the contact length of the triangular facet i of the soap film that is in contact with the object and $\vec{n}_i$ denotes the unit normal vector to the surface at (x_i, y_i, z_i), the mid-point of edge i (see figure 1c). Since the surface of the film contacts the object at 90°, it

applies a network torque, $\vec{\tau}^n$, on the object. Letting $\vec{r}_i = (x_i - x_0, y_i - y_0, z_i - z_0)$ denote the vector that connects the centre of the object with the midpoint of edge i, it is clear that $\vec{r}_i$ and $\vec{n}_i$ are in general not parallel when $\lambda > 2$. The network torque is calculated as the sum of vector cross-products

$$\vec{\tau}^n = 2\gamma \sum_i l_i \vec{r}_i \times \vec{n}_i. \tag{8}$$

Similarly, bubbles in contact with the object apply a pressure force, $\vec{F}^p$, over its surface and this is calculated by the summation

$$\vec{F}^p = -\sum_k p_k A_k \vec{n}_k, \tag{9}$$

where A_k denotes the area of the k-th triangular facet of the object, p_k refers to the pressure of the bubble adjacent to the facet k, and $\vec{n}_k$ denotes the outward unit normal vector positioned at the midpoint of this facet, say (x_k, y_k, z_k). Note that the negative sign is due to the fact that the bubble applies an inward push due to its pressure. As for the network force, there is a contribution from this pressure force towards a torque, $\vec{\tau}^p$. Let $\vec{r}_k = (x_k - x_0, y_k - y_0, z_k - z_0)$ denote the vector that connects the centre coordinates of the object with the mid-point of the k-th triangular facet of the object. The pressure torque is given by the summation

$$\vec{\tau}^p = -\sum_k A_k p_k \vec{r}_k \times \vec{n}_k. \tag{10}$$

Therefore the resultant force and torque exerted on the super-quadric object are

$$\vec{F} = -mg\vec{z} + \vec{F}^n + \vec{F}^p, \tag{11}$$

$$\vec{\tau} = \vec{\tau}^n + \vec{\tau}^p, \tag{12}$$

respectively, where $\vec{z}$ denotes the unit vector in the positive z direction. We will from now on use the component form of these forces, that is $\vec{F} = (F_x, F_y, F_z)$ and $\vec{\tau} = (\tau_x, \tau_y, \tau_z)$.

Each time step of a simulation involves equilibrating the soap film while the position and orientation of the object are fixed, calculating the forces it exerts on the object, and then moving the object in the direction of the resultant force by a small amount. We choose a small constant ε that sets the effective time-scale of our simulations. At each time step we move the object by $\varepsilon\vec{F}$ and rotate it by $\varepsilon\vec{\tau}$, using the standard right hand convention for rotation. We choose $\varepsilon = 1/400Bo$, which ensures convergence in the sense that the results do not change by making ε smaller. Rotating the object requires applying the matrix given

in eq. (6) where the angles of rotation around the x, y and z axes are $\phi_j = \varepsilon\vec{\tau}_x$, $\theta_j = \varepsilon\vec{\tau}_y$ and $\psi_j = \varepsilon\vec{\tau}_z$ respectively for the j-th time step, where $j = 1, 2, 3, \ldots$. Thus after n time steps, the orientation of the object is given by the 3×3 matrix

$$\mathbf{R} = \prod_{j=n}^{j=0} \mathbf{R}_j = \begin{pmatrix} r_{1,1} & r_{1,2} & r_{1,3} \\ r_{2,1} & r_{2,2} & r_{2,3} \\ r_{3,1} & r_{3,2} & r_{3,3} \end{pmatrix}. \tag{13}$$

The columns of this matrix can be thought of as the unit normal vectors that define the orientation of the super-quadric object, which we denote by $\vec{N}_1$, $\vec{N}_2$ and $\vec{N}_3$ respectively (see figure 1a). We will record the orientation of the descending object by determining the angles that these three vectors make with the vertical z-axis, which we denote by $\alpha_1 = \cos^{-1}(r_{3,1})$, $\alpha_2 = \cos^{-1}(r_{3,2})$ and $\alpha_3 = \cos^{-1}(r_{3,3})$ respectively.

At each time step, the soap film is at equilibrium. We accept that an equilibrium state has been reached when the energy of the soap film has converged to within a tolerance of 1×10^{-5}, using a combination of gradient descent and conjugate gradient minimization iterations. It can take up to 10,000 iterations of these numerical methods to reach the given tolerance. The iterations are interspersed with upkeep of the tessellation and checks for soap film detachment. We also apply small perturbations to the surface of the soap film during the equilibration process by jiggling the vertices slightly. In this case, a random displacement is applied to each vertex independently using a Gaussian distribution with a deviation of 0.02 times the mean edge length of the triangular mesh [16]. This perturbation was found to be robust enough to optimize the process of reaching a minimum energy for the soap film under the given constraints.

III. RESULTS

Although the simulation that we model is relatively simple, it provides a rich system to study the interaction between a descending object and a soap film as we can vary many parameters. In this section, we summarise the results of varying the radius of the cylindrical container and the shape, initial orientation and position of the object.

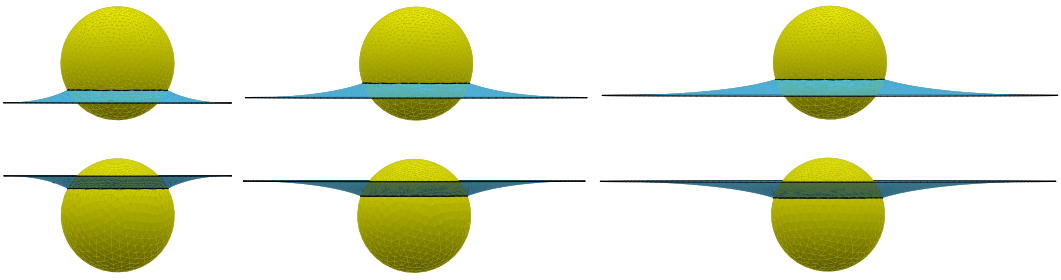

(a)

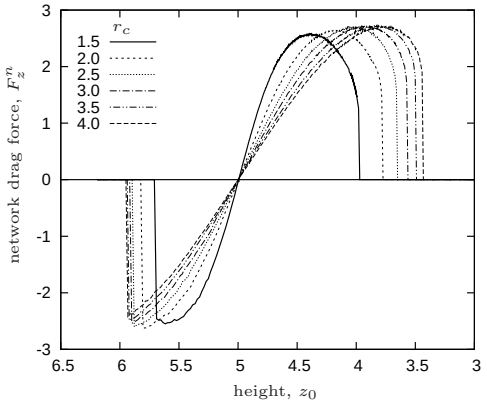

(b)

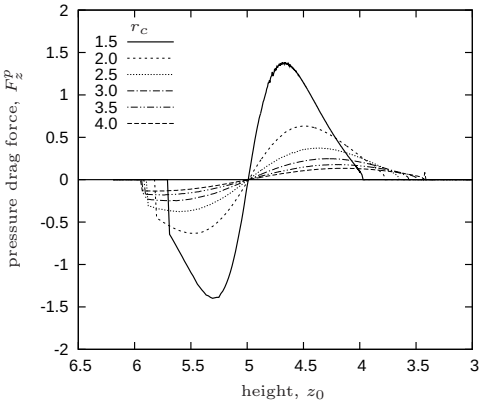

(c)

FIG. 2: Variation of the radius, r_c, of the cylindrical container: (a) Snapshots of the simulation when a sphere reaches heights of $z_0 = 5.5$ (top row) and $z_0 = 4.5$ (bottom row) as it falls through a soap film contained in a cylinder with radius $r_c = 2, 3, 4$ (from left to right respectively). The height of the centre of the sphere matches the height of the film on the boundary of the cylinder when $z = 5$. The drag force exerted by the foam on the object is plotted versus the height of the sphere, and is split into a (b) network contribution and a (c) pressure contribution.

A. Variation of tube radius

Let us first consider the effect that varying the radius of the cylindrical container has on the interaction between a soap film and a descending *spherical* object. We set the radius of the sphere and the Bond number to one, and initially position it at the centre of the cylinder above the soap film. We vary the radius of the cylindrical container between $r_c = 1.5$ and $r_c = 4$ in increments of 0.5, and probe how the soap film is perturbed by the sphere and the forces exerted on the object in each case.

Figure 2a shows how a film is perturbed when it contacts a sphere that is at a height of $z_0 = 5.5$ (after attachment) and $z_0 = 4.5$ (before detachment) for a cylindrical container with radius $r_c = 2, 3, 4$, increasing from left to right. Note that the film lies at a height of $z = 5$ when its height matches that of the sphere. Two things stand out from these images: (i) The height of the contact line of the film with the container increases in range when decreasing the radius of the container. This is a direct consequence of the bubble volume constraints we set, and the smaller the radius of the tube, the more the film has to move relative to the descending sphere to satisfy these constraints. (ii) The mean curvature of the film decreases when increasing the radius of the container. Since the soap film contacts both the sphere and the wall of the container at ninety degrees, its curvature must decrease when we increase the tube radius. It follows from the Laplace-Young law that the pressure differences across this film decreases when we increase the radius of the container. Thus, the resultant pressure drag force exerted on the sphere from the contacting bubbles decreases in magnitude for increasing tube radius (as shown in figure 2c).

The network drag force applied by the soap film on the sphere is shown in figure 2b. Film attachment to the sphere is shown by the sharp negative jump in the network drag as the film pulls the sphere downwards at this stage. The network drag force then increases as the sphere descends. It is equal to zero when $z_0 = 5$, that is when the height of the sphere matches that of the film, and the film is perfectly horizontal (not shown). The film then becomes perturbed again as the sphere falls further, so that it applies a positive (upward) network drag on the sphere, resisting its downward motion. The network force goes to zero again when the film detaches from the sphere. The magnitude of the network drag force after attachment and before detachment of the film from the sphere is unchanged for all values of the tube radius that we consider. The heights of the sphere at which film attachment and detachment occur depends on the radius of the tube, as has already been explained to be the consequence of the bubble volume constraints.

The pressure contribution to the drag force that the foam exerts on the sphere is in the same direction as the network contribution (see figure 2c). Unlike the network contribution, the magnitude of the pressure drag force increases when decreasing the radius of the cylindrical container: The pressure contribution to the drag force is around half the network contribution when $r_c = 1.5$ but decreases to around a tenth of the network contribution when $r_c = 4$.

In the sections that follow, we keep the radius of the cylindrical container fixed at $r_c = 4$ so that we can assume that the pressure forces applied on a descending object are small compared to the network forces.

B. Variation of shape

We now vary λ, the shape parameter from equation 1. We consider values between $\lambda = 2$ (a sphere) and $\lambda = 20$ (a cube with smooth rounded edges and corners). The initial orientation of the object is constant throughout this section, with the angles used for setting up its orientation all set to zero so that a cube presents a flat face to the soap film. The object is free to rotate as it falls through the soap film. The initial position of the object is again set so that its centre coordinates lie at $x_0 = y_0 = 0$ and $z_0 > 6$, so that it is at the centre of the cylinder and above the soap film.

We focus on the deformation caused to the soap film by the descending object, and the forces exerted by the soap film on the object as a result. Snapshots of the simulation just after the film attaches itself to the descending object and just before it detaches are given in figure 3a. These show how the deformation differs for three examples; a sphere ($\lambda = 2$), an object that is between a sphere and a cube ($\lambda = 4$) and a cube with smooth rounded edges ($\lambda = 20$).

The shape of the descending object clearly affects how the soap film deforms directly after attachment, as shown in the top row of images in figure 3a. Since the contact angle between the film and the object is 90°, the contact line between the soap film and the object after attachment is highest for the sphere. In this case, the film has to bend upwards the most to reach its energy minimum under the given boundary conditions and volume constraints. For the more cubic objects (where $\lambda = 4$ and $\lambda = 20$), the soap film is not perturbed as much after attachment, and does not have to bend as much upwards to satisfy the boundary conditions. As λ is increased, the vertical faces of the object become flatter, and therefore the soap film does not need to rise as far during the equilibration process. As a result, the perturbation caused to the soap film directly after attachment decreases with increasing values of λ.

Conversely, it is clear from the bottom row of images in figure 3a that the soap film's deformation prior to detachment from the object increases with λ. The rounded shape of a

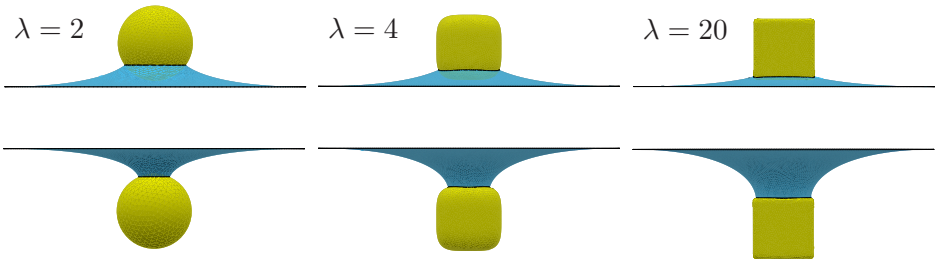

(a)

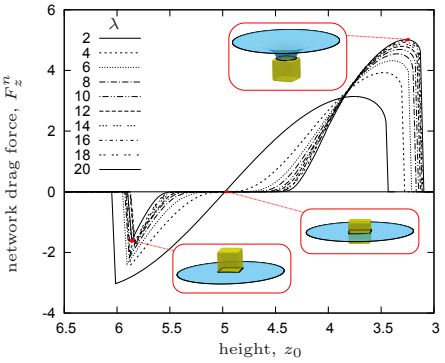

(b)

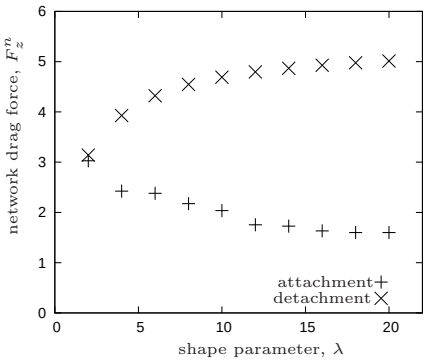

(c)

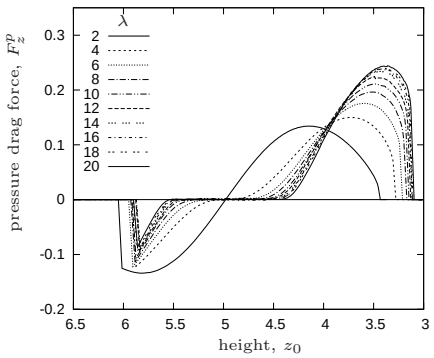

(d)

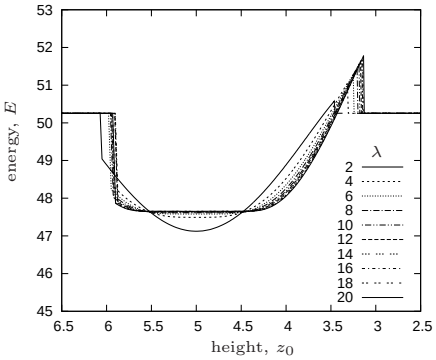

(e)

FIG. 3: Variation of the shape parameter λ: (a) A side view of the simulation after attachment of the soap film to the object (top) and before detachment of the soap film from the object (bottom) for $\lambda = 2$, 4 and 20 (from left to right). These images have been positioned so that the height of the film matches for each row, and so should not be used to compare the position of the object. (b) The network drag force, F_z^n, exerted on the objects as they fall through a soap film versus their height, z_0. The inset snapshots indicate the position of a cube with $\lambda = 20$ for different values of z_0. (c) The maximum (absolute) value of the network drag force exerted on the object by the soap film after attachment and before detachment. (d) The pressure drag force, F_z^p, exerted on the object and (e) the energy E (i.e. surface area) of the soap film versus the height of the object, z_0.

sphere means that the contact line of the soap film moves steadily up over its surface as the sphere descends, resulting in the earliest detachment. For the more cubic objects, the film comes into contact with the rounded edges that surround the upper face of the object prior to detachment. Here, the film does not have to move very far to retain its 90° contact angle with the object while still satisfying the volume constraints. This is particularly true when λ is high, where the curvature of the rounded edges is large. As a result, the film stays in contact with the rounded edge of the cube for longer, becoming more stretched as the cube descends. In fact the film bends downwards so much when $\lambda = 20$ that it is near vertical at its contact line with the object (see figure 3a, bottom right). The film detaches from a cubic object once it has moved past the rounded edges and corners and onto the upper (horizontal) face.

Figure 3b shows how the network drag, $\vec{F}_z^n$, varies with the height of the super-quadric object in the cylinder for different values of λ. The attachment of the soap film to the object is evident in figure 3b by a sharp negative (downward) network drag, which is a result of the angle that the soap film makes with the vertical axis as it contacts the object. The magnitude of the network drag just after the soap film attaches itself to the solid object decreases slightly for increasing λ (see figure 3c). This can be explained by the fact that the angle made between the vertical direction and the soap film over its contact length with the object increases with λ, and therefore the contribution of the network force towards the drag reduces.

Once the soap film is attached to the object, the network force increases to zero when the height of the object's centre is aligned with the height at which the soap film contacts the cylinder wall (see figure 3b). Once the object passes this point, the network force becomes positive, thus contributing to resisting the downward motion of the object. The maximum value of the network drag is achieved for the most cubic object (where $\lambda = 20$). Note also that the interval of height where the object is in contact with the soap film increases with λ. This is a result of the soap film's contact line with the object becoming more stagnant on the rounded edges of the cube's upper face. As these rounded edges become more curved as λ increases, the minimal surface remains in contact with the edges for longer, and the soap film becomes more stretched in the vertical direction before detaching from the object. This result is confirmed in figure 3c, which shows that the absolute value of the network drag instantaneously before the soap film detaches from the object increases with λ. We propose

that under the given conditions, the network drag tends to $2\pi r_s$ as λ increases without bound (for a surface tension of $2\gamma = 1$). This is the circumference of the largest circle that can be inscribed within the upper square surface of the cube. Once the film is no longer contacting the rounded edges of the cube, its surfaces slips along the upper flat surface of the cube before detaching.

The pressure drag, $\vec{F}_z^p$, versus the height, z_0, of the object in the cylinder is shown in figure 3d for the same set of values of λ. As we discussed in the previous section, the pressure contribution to the drag force is an order of magnitude smaller than that of the network force when $r_c = 4$, and they both act in the same direction. This was also seen to be the case in previous work by Davies and Cox [15]. For a sphere, the pressure drag exhibits symmetry between attachment and detachment. This is not the case for objects where $\lambda > 2$. Recall that the pressure force depends on the pressure *difference* between the two bubbles, and therefore the curvature of the film that separates them. After attachment, the curvature of the soap film is such that the pressure in the lower bubble is less than the pressure of the upper bubble. In this case, the pressure drag force is negative during the attachment (and therefore it contributes to drag the object downwards). As for the network force, it increases to zero when the centre of the object is perfectly aligned with the position of the soap film. This is to be expected as the shape of the soap film is such that its overall curvature is zero here, and therefore the pressure difference between the two bubbles is zero. As the object descends further, the curvature of the soap film switches sign so that the pressure drag becomes positive, increasing until reaching a maximum value just before detachment. The maximum pressure drag exerted increases with λ in a similar fashion to the network contribution to the drag force.

Figure 3e shows how the surface area of the soap film varies with the height of the object in the cylinder for different values of λ. Before the soap film attaches to the object, its area is simply $2\pi r_c$. That area sharply decreases after the soap film attaches itself to the object, reaching a minimum when the height of the centre of the object is perfectly aligned with that of the soap film. The cross-sectional area of the object is at its largest here for all values of λ, and therefore it is to be expected that the minimum energy is attained here. The soap film is then stretched by the object as it falls beyond this point, with a maximum energy reached just before detachment. Again, is is clear from this figure that the amount of film stretching required before detachment increases with λ.

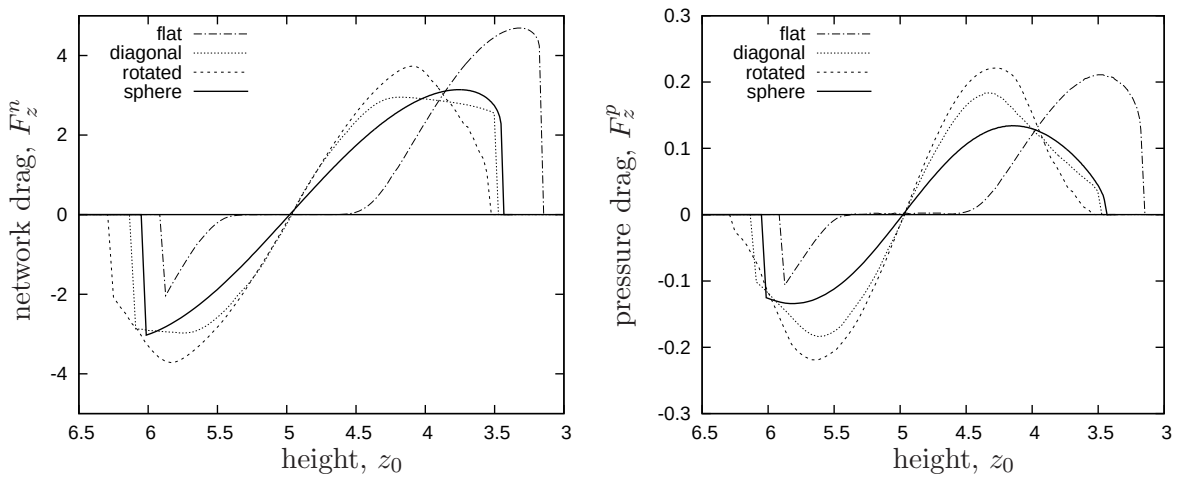

(a) (b)

FIG. 4: The drag force exerted on a cube descending through the centre of a soap film in three orientations: a *flat* orientation where the angles between the normal vectors defining the cube, $\vec{N}_1$, $\vec{N}_2$ and $\vec{N}_3$ and the z axis are $\alpha_1 = \alpha_2 = \pi/2$ and $\alpha_3 = 0$ respectively, a *diagonal* orientation where $\alpha_1 = \alpha_2 = \pi/4$ and $\alpha_3 = \pi/2$, and a *rotated* orientation where $\alpha_1 = \alpha_2 = \alpha_3 = \pi/2 - \tan^{-1}\left(1/\sqrt{2}\right)$. The drag force is separated into (a) a network component, F_z^n, and (b) a pressure component, F_z^p, and plotted versus the height, z_0, of the object in the cylindrical container. Note that the forces exerted on a sphere are also included for comparison.

C. Variation of initial orientation

In this section we inspect how the orientation of the object affects how it perturbs a soap film that it falls through. We investigate whether or not a bamboo foam can be used to re-orient a cubic object in a controlled and predictable way. To isolate the effect of the object's orientation, we keep the shape parameter of the object fixed at $\lambda = 10$. We vary the initial orientation of the cube by choosing different values for ϕ_0 and θ_0, the angles by which the object is rotated around the x and y axes during the initial setup respectively. We keep ψ_0, the angle of rotation around the z axis, equal to zero, and allow the cube to fall from the centre of the cylinder.

1. Stable orientations

Let us first consider three initial orientations of the cube which do not change as the cube falls through the centre of the soap film. In fact we have already considered the first of these orientations in the previous section. In that case the angles between the normal vectors $\vec{N}_1$, $\vec{N}_2$ and $\vec{N}_3$ and the z axis are $\alpha_1 = \alpha_2 = \pi/2$ and $\alpha_3 = 0$ respectively (as shown in figure 1a). We call this the *flat* orientation.

The *diagonal* orientation has $\alpha_1 = \alpha_2 = \pi/4$ and $\alpha_3 = \pi/2$.

In the *rotated* orientation all three normal vectors have the same angle with the z axis, that is $\alpha_1 = \alpha_2 = \alpha_3 = \pi/2 - \tan^{-1}\left(1/\sqrt{2}\right)$. These three orientations are shown in figure 5 just after soap film attachment. Their stability when the cube falls through the centre of the foam can be explained by symmetry: the deformation of the soap film will be symmetric around the z axis, meaning the torque will be negligible. In fact, we will show later that the *flat* orientation is the only stable orientation for a cube descending down the centre of a bamboo foam, and that the *diagonal* and *rotated* orientations are meta-stable.

Figure 4 shows the drag force the soap film exerts on the cube in these three orientations. The network component of the drag force is shown in figure 4a, which demonstrates the importance of the object's orientation to the forces it experiences. The negative drag that the soap film exerts instantaneously after attaching itself to the cube is smallest in magnitude for the cube in the rotated orientation, where the soap film finds its minimal area without deforming as much, only needing to engulf the leading apex of the cube. The initial network force exerted on the cube in the diagonal orientation is larger in magnitude than for any other orientation, as in this case the soap film contacts the object over a greater length than for the rotated cube and at a larger angle to the horizontal than for the cube in the flat orientation (see figure 5).

As the cube falls further, the downward network force increases to its largest magnitude for the cube in the rotated orientation, for which the cross-sectional area to be navigated by the soap film is largest. The negative network drag is also greater in magnitude for the cube in the diagonal orientation compared to the flat orientation, as the angle the soap film makes with the horizontal here while contacting the cube is larger. The network drag then increases to zero as z_0 approaches the vertical position of the soap film. Here, the soap film becomes completely horizontal for a cube in the diagonal and flat orientations. However, for

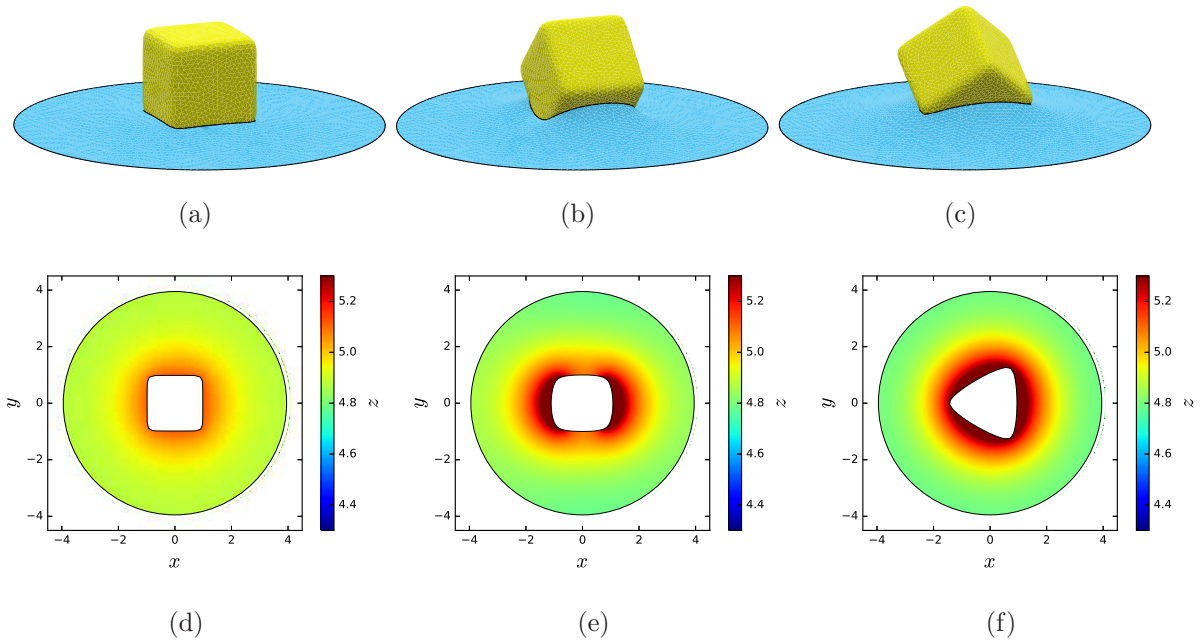

FIG. 5: Snapshots of the simulation when a cube (with $\lambda = 10$) in the (a) *flat*, (b) *diagonal* and (c) *rotated* orientation reaches a height of $z_0 \approx 5.9$ in the centre of the cylinder, thus contacting and deforming the soap film. The shape of the surface of the film for these three cases is visualized by surface plots directly below the snapshots in (d), (e) and (f) respectively, with the height of the film indicated by colour.

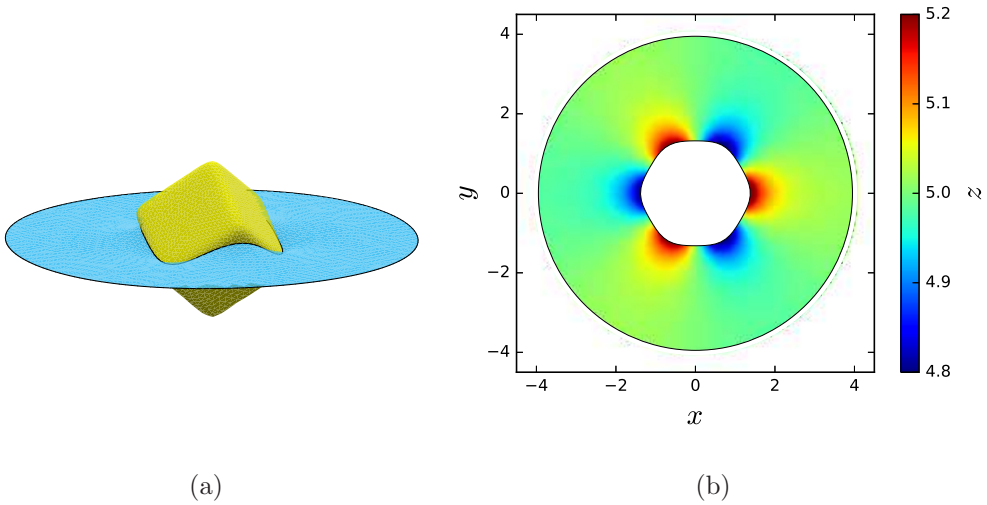

FIG. 6: (a) Snapshot of the simulation and a (b) surface plot of the soap film where the height of the centre of the cube in the *rotated* orientation is aligned with the height of the soap film.

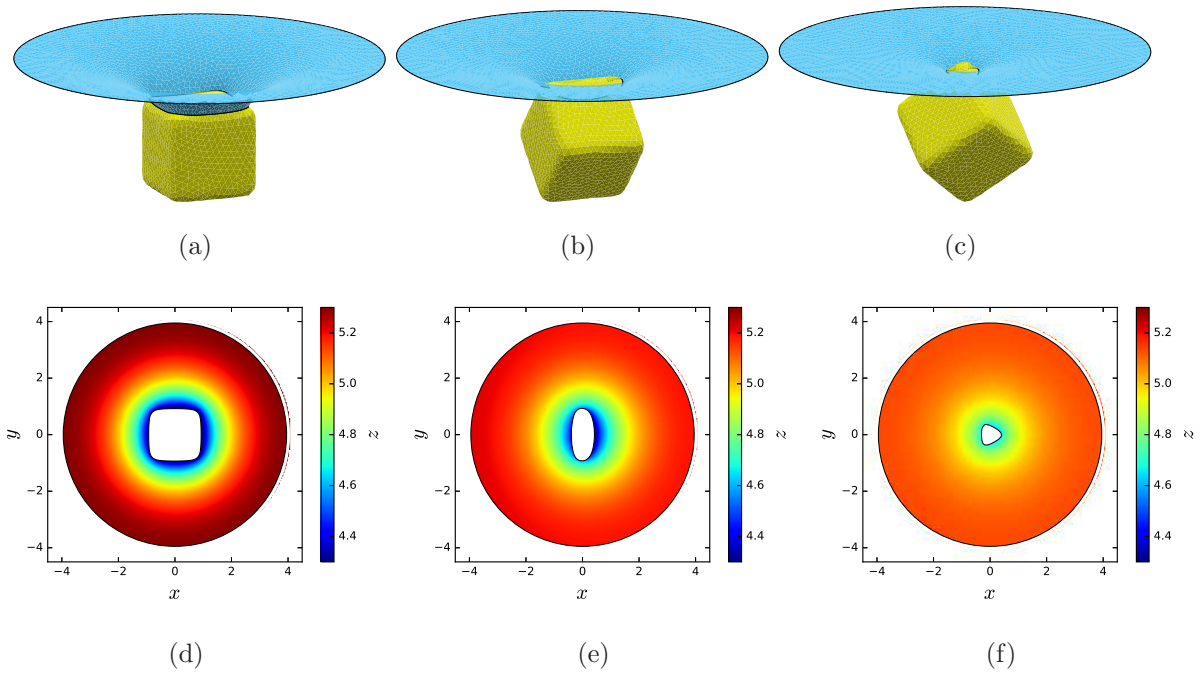

FIG. 7: Snapshots of the simulation where a cube in the (a) *flat*, (b) *diagonal* and (c) *rotated* orientation reaches a height of 3.5 in the cylinder, thus approaching the point at which the soap film detaches. The shape of the soap film for these three snapshots is visualized by the surface plots in (d), (e) and (f) respectively, with the height of the surface denoted by colour.

the cube in the rotated orientation it takes a hexapolar deformation that includes three rises and three depressions that are symmetric around the z-axis (see figure 6). This deformation was seen for a cube in thin films in the work of Morris *et al.* [28] and for cubes lying at fluid-fluid interfaces in the work of Soligno *et al.* [33].

The forces exerted on the cube by the soap film just before detachment vary considerably with the orientation of the object, as shown in figure 4a. In this case, the network drag exerted on the cube in the rotated and diagonal orientations is smaller in magnitude than for the cube in the flat orientation. Leading up to detachment, the soap film surrounds only one corner of the cube in the rotated orientation, compared to two corners for a cube in the diagonal orientation and four corners for a cube in the flat orientation. As a result, the soap film's catenoid-like shape has a thinner neck leading up to detachment from a cube in the rotated orientation. Therefore the instability that triggers the film to detach from a cube happens sooner when a cube is in the rotated orientation compared to the diagonal and flat

orientations, for which the neck of the soap film catenoid is wider. This is shown to be the case in figure 7, which includes snapshots taken from the three simulations just before the soap film detaches from the cube.

More insight can be gained by looking at how the pressure drag force varies with the height of the cube in the cylinder (see figure 4b). The most striking result here is how antisymmetric the pressure drag force is between when the soap film attaches to and detaches from the cube for the rotated and diagonal orientations. For these orientations, the deformation caused to the soap film by the cube is close to being symmetric about the point at which the centre of the cube is perfectly aligned with the height of the soap film. Note that the direction of the curvature of the film's surface just before detachment is the opposite of the direction of curvature after attachment, and that the similarity between the geometry of the film does not extend to the instances directly after attachment and before detachment (as shown in figures figures 5e,f and 7e,f). We previously discussed how the soap film deformation was not symmetric at all for the cube in the flat orientation, and this is reflected in the forces exerted on it by the soap film.

2. Unstable orientations

Let us now consider initial orientations for the cube which cause the soap film to deform in a non-symmetric way, and therefore where the torque exerted by the foam becomes non-negligible. We first consider initial orientations which are set by rotating the cube around only one axis. Here we fix $\phi_0 = \psi_0 = 0$ and vary θ_0 between zero and $\pi/2$. In this case, the angle α_1 is initially equal to $\pi/2$ while α_2 is varied and $\alpha_3 = \pi/2 - \alpha_2$. Figure 8a shows how the orientation of the cube, given in terms of α_2, varies as the cube descends through the soap film. Note that when α_2 is initially zero or $\pi/2$, the cube is in the *flat* orientation, which we investigated in the previous section. The stability of this orientation is confirmed here by the fact that α_2 does not change with the height of the cube in both cases. Similarly, when the initial value of α_2 is $\pi/4$, we have the *diagonal* orientation, and again the angle recorded here does not change as the cube interacts with the soap film.

The new and interesting result here is what happens in between these two orientations. As expected from symmetry, the results for $\alpha_2 = 0.1\pi$ and $\alpha_2 = 0.4\pi$ are equivalent, as are the results for $\alpha_2 = 0.2\pi$ and $\alpha_2 = 0.3\pi$. In all of these cases, when the soap film attaches

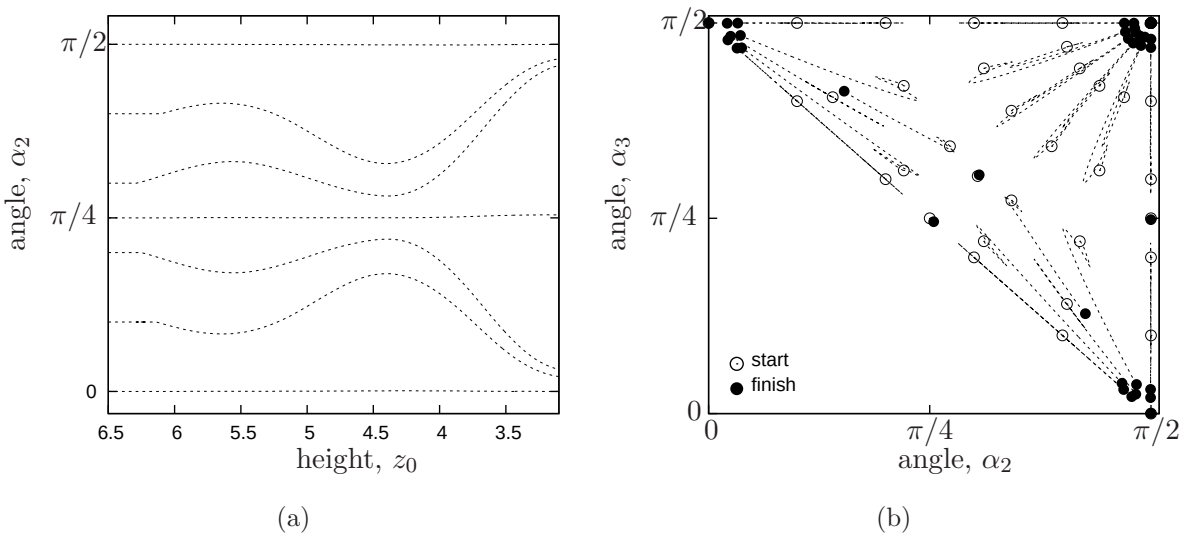

FIG. 8: Variation of the orientation of a cube (with $\lambda = 10$): (a) The variation in the angle α_2 (from various initial values) versus the height of the cube in the cylindrical tube, where α_1 is initially set to $\pi/2$ and therefore $\alpha_3 = \pi/2 - \alpha_2$. (b) Here, we consider many initial orientations of the cube by considering every possible pairwise combination of ϕ_0 and θ_0 from the set of values $\{0, 0.1\pi, 0.2\pi, 0.3\pi, 0.4\pi, 0.5\pi\}$. The orientation of the cube is plotted in terms of the angle α_2 versus α_3. An empty circle represents the starting orientation of the cube, a dashed line shows how the orientation varies throughout the simulation and the filled circle shows the final orientation of the cube after it has detached from the soap film.

itself to the cube it exerts a slight non-zero torque that acts to rotate the object towards the *flat* orientation. Here, the soap film moves above the lowest side of the cube's lower face, but remains below the opposite edge of the same face (see figure 9a). As a result the shape of the soap film is not symmetric around the z-axis, as shown in figure 9d. In figure 9a, the contribution to the torque exerted by the film on the cube is largest on the right hand side, where the film reaches its highest point. This contributes to rotate the cube in figure 9a in the clockwise direction, and therefore towards the *flat* orientation. This is cancelled out by an opposite torque that occurs after the cube falls further and its centre coordinates become closer to the vertical position of the soap film. It is shown in figure 9b and 9e that the film is slightly higher on the opposite side to what it was previously. However, as the soap film slips further along the surface of the cube the torque that the foam exerts increases dramatically. The soap film slips towards the rounded edge of the cube that surrounds its

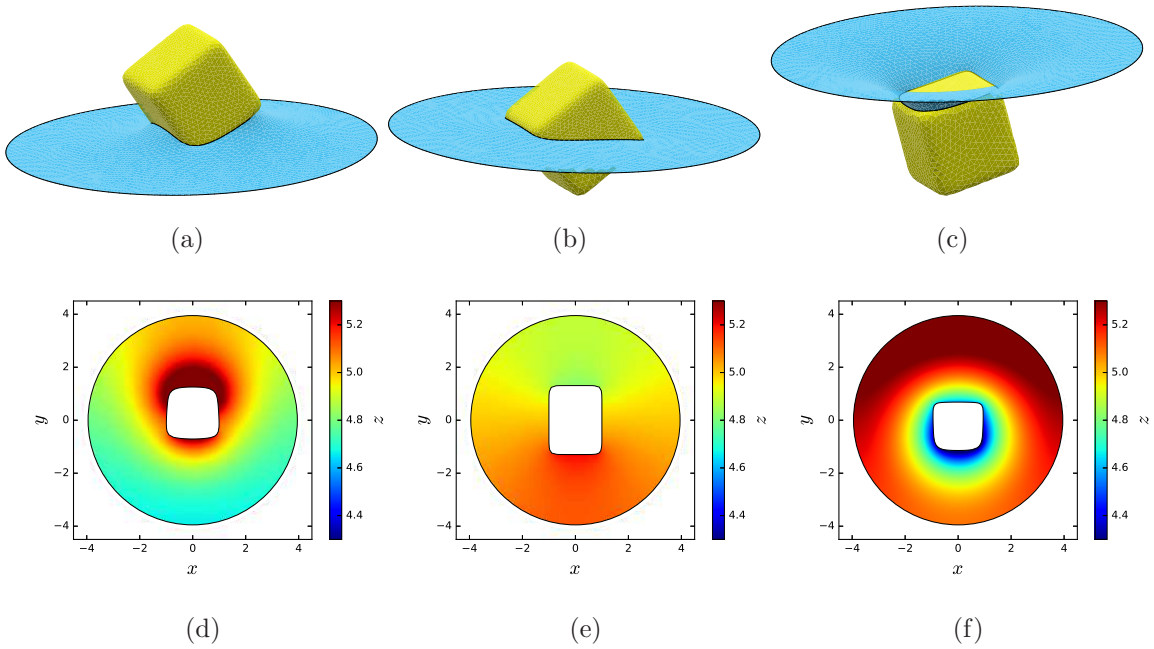

FIG. 9: Snapshots of the simulation when the centre of a cube that is initially oriented so that $\alpha_1 = 0.5\pi$, $\alpha_2 = 0.3\pi$ and $\alpha_3 = 0.2\pi$, reaches a height of (a) $z_0 \approx 6$, (b) $z_0 \approx 5$ and (c) $z_0 \approx 3.5$. The shape of the soap film for these three snapshots is visualized by the surface plots in (d), (e) and (f) respectively, with the height of the surface denoted by colour.

upper face (see figures 9c and f). The film is in contact with this rounded edge for many time steps, exerting a network torque that in effect rotates the cube strongly towards the flat orientation. For example, in figure 9c, the contribution to the torque is much higher from the left hand side as the film contacts the cube nearly vertically here, thus applying a large upward pull on this side. It is clearly shown in figure 8a that the *flat* orientation is the most likely outcome of dropping a cube that has been rotated around only one axis through a soap film, and that it is the highly non-symmetric deformation of the soap film that occurs before detachment that is the main driving force for this result.

We now vary the values of both the angles ϕ_0 and θ_0 used to set the initial orientation of the cube, doing so in increments of $\pi/10$ between zero and $\pi/2$, considering every possible combination. Figure 8b shows how the orientation of the cube changes as it interacts with a soap film. Here, the angles that two of the normal vectors that define the cube make with the z axes are plotted against each other. The stable orientations are the ones where the cube doesn't rotate as it falls through the soap film. This is the case when the angles (α_2, α_3) are

equal to $(0, \pi/2)$, $(\pi/2, 0)$ and $(\pi/2, \pi/2)$, which are all representations of the *flat* orientation. It is also the case when $(\alpha_2, \alpha_3) = (\pi/4, \pi/4)$ and $(\pi/2, \pi/4)$, which are two representations of the cube in the *diagonal* orientation. We also include the result for the *rotated* orientation that we previously discussed, which is shown at $\left(\pi/2 - \tan^{-1}\left(1/\sqrt{2}\right), \pi/2 - \tan^{-1}\left(1/\sqrt{2}\right)\right)$ here. All other initial orientations are unstable. It is shown in figure 8b that the orientation of the cube in these unstable orientations also changes in a zigzag manner: The cube is initially rotated towards the flat orientation after film attachment, and then it is rotated in the opposite direction for a short period before being rotated towards the flat orientation again leading up to film detachment. As previously discussed, the forces exerted by the film on the object leading up to detachment are dominant in setting the final orientation of the object. This is shown by the large collection of filled circles at the three corners that represent this orientation in figure 8b. It is clear from this figure that unless the cube is initially in the *rotated* or *diagonal* meta-stable orientations, then it is highly likely to be reoriented to the flat orientation as it falls through the centre of a soap film.

D. Variation of initial position

So far we have considered what happens when a super-quadric object falls through the centre of a horizontal soap film contained in a cylindrical tube. We now vary the initial position of the object in the cylinder and inspect how its radial position varies as it interacts with the soap film it falls through. We vary the initial radial distance, $r_{xy} = \sqrt{x_0^2 + y_0^2}$, between the centre of the object and the centre-line of the cylinder (where $x = 0$ and $y = 0$) by varying x_0, the x coordinate of the object's centre. A simulation is terminated once the descending object comes into contact with the boundary of the cylinder container.

Figure 10 shows how the radial position of the object changes as the object interacts with a soap film, starting from different initial positions. When a sphere is allowed to fall through a horizontal soap film from an off-centre position in the cylinder, the effects of the asymmetry of the deformation to the film are weak (see figure 10a). There are small increases in r_{xy} as the sphere falls through the soap film, so that its path deviates slightly towards the wall of the cylinder. This tendency becomes more apparent the further the sphere is away from the centre of the cylinder initially. If the sphere fell through a long bamboo foam containing many bubbles, it would eventually fall towards the wall of the cylinder, and the

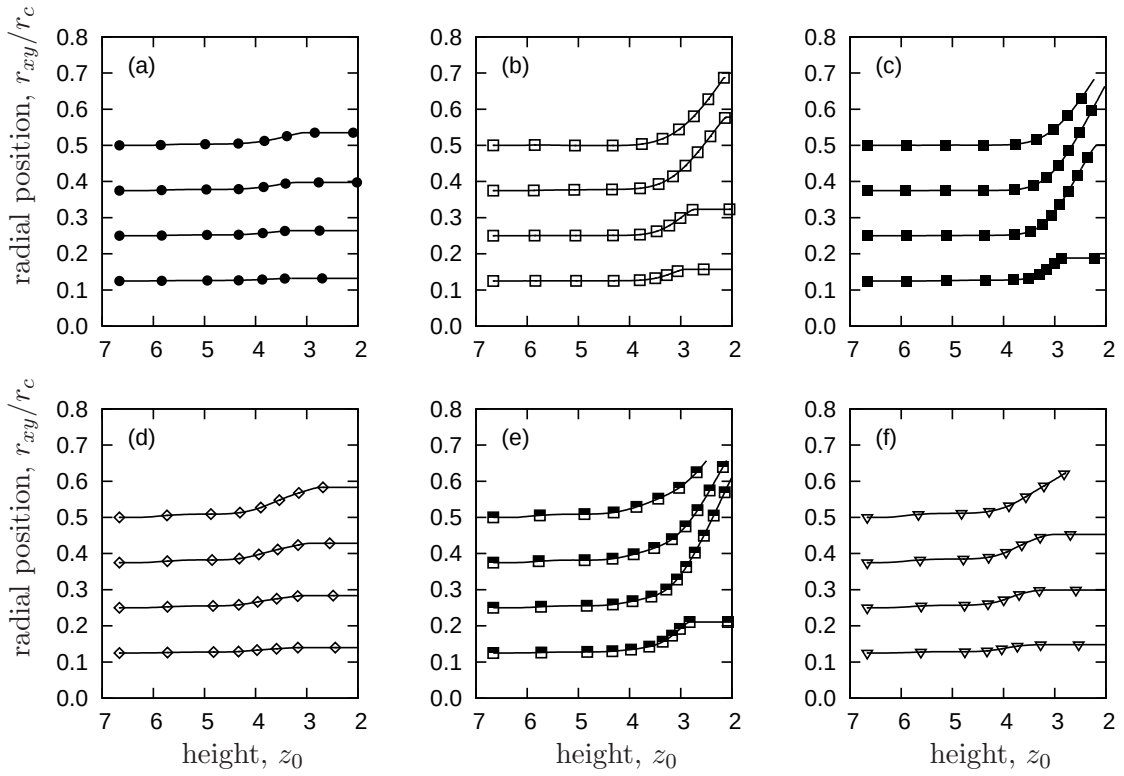

FIG. 10: Variation in the radial position, $r_{xy}/r_c = 0.25\sqrt{x_0^2 + y_0^2}$, of objects versus their height in the foam, with points included every 40 time steps. Four initial positions are considered: $r_{xy}/r_c = 0.125$, 0.25, 0.375, 0.5 for (a) a sphere, (b) a cube in the *flat* orientation with $\lambda = 6$, (c) a cube in the *flat* orientation with $\lambda = 10$, (d) a cube in the *diagonal* orientation with $\lambda = 10$ where the nearest face to the side of the cylinder is vertical, (e) a cube in the *diagonal* orientation with $\lambda = 10$ where the nearest faces to the side of the cylinder are slanted and (f) a cube in the *rotated* orientation with $\lambda = 10$.

foam would not control its motion.

Figures 10b and 10c show how the radial position of cubes in the flat orientation, with $\lambda = 6$ and $\lambda = 10$ respectively, varies with their height. It is clear here that the effects of positioning the cube off-centre in the cylinder are stronger than for a sphere. The radial distance of the cube from the centre of the cylinder deviates more here, especially just before it detaches from the soap film, which causes the cube to fall towards the wall of the cylinder. We also note that this effect is stronger for the largest value of λ, where the deformation caused to the soap film is greater.

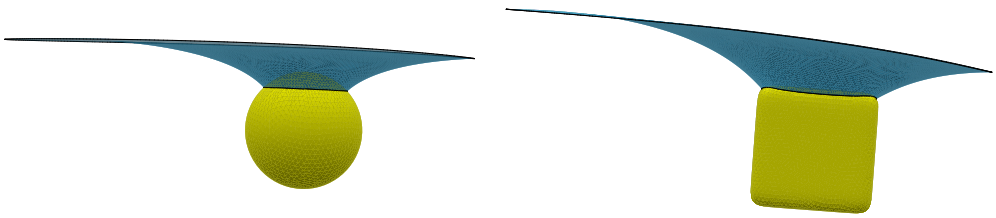

(a) (b)

FIG. 11: Snapshots of simulations where (a) a sphere and (b) a cube (initially) in the flat orientation fall through a soap film from an off-centre position in the cylinder, causing non-symmetric deformation to the soap film.

An indication of why wall effects are more prevalent for a cube compared to a sphere is offered in figure 11. The angles that the soap film makes with the horizontal as it contacts the cube from the left and the right are clearly different, which is not the case for the sphere. On the side of the cube that is nearest to the cylinder wall (to the left in figure 11), the soap film makes a smaller angle with the horizontal than on the other side of the cube. As a result, there is a resultant network force that drags the cube further towards the nearest wall. We also note that the unbalanced deformation of the soap film also tilts the cube slightly, which indicates that the *flat* orientation is no longer stable when the cube is positioned off-centre in the cylinder. The deformation is more symmetric for the sphere, explaining why it deviates less from a vertical path compared to the cube.

Figures 10d and 10e show that a cube in two different *diagonal* orientations also move towards the nearest wall when positioned off-centre in the cylinder. Two different representations of the *diagonal* orientation are considered: one in which the cube has a vertical face nearest to the wall and the other where the cube has two slanted faces nearest to the wall. It is clear from figure 10d that the effect the asymmetric deformation has on the motion of the cube is weaker for the first case than for the second diagonal orientation shown in figure 10e. When the cube has two slanted faces nearest to the wall, the film between the

object and the wall comes into contact with a (horizontal) rounded edge of the cube. The angle the soap film makes with the horizontal plane at this stage is close to zero, therefore it pulls the object towards this nearest wall with a large network force. This is similar to what happens in figure 11b for the cube in the flat orientation. The effect is weaker for a cube in the diagonal orientation in which it has a vertical face close to the wall, and the film moves steadily along this face as the cube falls. This is also the case for the cube in the rotated orientation (see figure 10f), where the attraction towards the wall is of a similar nature to that experienced by a cube in the diagonal orientation considered in figure 10d. This again demonstrates that the soap film navigates the surface of the cube in the rotated orientation without deforming as much, especially leading up to detachment, where the forces are at their largest.

IV. CONCLUSIONS

We have presented results of 3D quasi-static simulations in which a light solid object defined by a super-quadric equation falls under gravity through a horizontal soap film of a bamboo foam. We discussed in detail how the soap film deforms as it attaches to the object and prior to when it detaches from the object. The influence the soap film has over the final position and orientation of the solid object has also been discussed in detail. In particular, we investigated how the forces a soap film exerts on the object vary when we change the radius of the cylinder container, and the shape, orientation and initial position of the object.

Varying the radius of the cylinder does not change the magnitude of the network force exerted by the soap film on a sphere. However the pressure contribution to the drag force increases considerably with decreasing tube radius. For example, the pressure contribution to the drag force on a sphere with radius $r_s = 1$ is around half the network contribution when the radius of the cylinder is $r_c = 1.5$. When the radius of the tube is $r_c = 4$, the pressure force is an order of magnitude smaller than the network force. Thus, the downward motion of an object is slower in a foam contained in a thinner tube, meaning that the soap film can manipulate the position and orientation of the object for longer before detachment occurs.

It is clear that the shape of the object is pivotal in how the soap film deforms and the resulting forces that it exerts on the object. We found that both the network and pressure

drag force exerted on the object by the film increase with the shape parameter λ. This implies that a cube causes the soap film to deform much more than a sphere. This is particularly true in the build up to when the soap film detaches from the object, where it becomes much more stretched for a cube than it does around a sphere. In general, it takes the soap film more time to navigate surfaces with very high curvature such as the rounded edges of our cubes, especially when those edges are adjacent to flat surfaces that are perpendicular to the direction of the motion of the object. In these instances, the shape of the descending object acts to keep the neck of the catenoidal shape of the soap film wide enough to remain stable for longer.

Another important factor that determines how a film interacts with a solid object is the orientation of the object as it comes into contact with it. We considered many orientations of the cube and investigated the deformation to the soap film and the forces it exerts on the object. For a cube dropped centrally through the film, the *flat* orientation was the only stable orientation found, while the *diagonal* and *rotated* orientations were meta-stable. In all three cases, the deformation to the soap film remains symmetric around the centre-line of the cylindrical container, meaning that the network and pressure torques exerted by the foam remain negligible throughout. The deformation of the soap film is clearly different for these three orientations, in particular during attachment and detachment and this has been explained using geometrical arguments. For other initial orientations, the symmetry of the soap film deformation is broken, and therefore a non-zero torque is exerted by the foam. This is such that a cube not initially in one of the three aforementioned orientations is likely to be realigned by the horizontal soap film towards the *flat* orientation. The major contribution to this realignment occurs when the forces are at their greatest, that is as the soap film reaches the upper half of the object and before detachment.

Finally we investigated the effect of positioning the descending object off-centre in the cylindrical container. This also broke the symmetry of the soap film's deformation, resulting in the object being pulled towards the nearest wall of the cylinder by the soap film. This wall effect was seen to be strongest for a cube in the flat orientation, for which the soap film is perturbed the most, and weakest for a sphere or a cube in the rotated orientation for which a soap film is perturbed the least.

We propose that our results can be generalised to predict what happens when a solid object falls through a bamboo foam with many bubbles. Our results apply as long as the

bubbles are large enough so that the object is in contact with (at most) one film at any given time. Assuming that an object free falls when it is not in contact with a soap film, we predict that a cube in the flat orientation will descend through a bamboo foam slower than a sphere, or a cube in the diagonal and rotated orientations. We also predict that if a cube falls down the centre of a bamboo foam, then it will emerge at the bottom in the flat orientation, provided that it was not initially in the diagonal or rotated orientations. This may not be the case if bubbles are small enough so that an object can be in contact with more than one soap film at a time. We predict that a second film contacting the object may resist its re-orientation as it falls down the centre of a bamboo foam, as the two films would apply torques in opposite directions when contacting the object from above and below respectively.

We conclude that a bamboo foam may provide a good tool for precisely reorienting an object that falls through it from a central position in the cylindrical container. However, a bamboo foam does not provide good control over the motion of objects when they are positioned off-centre in the cylinder as the objects fall towards the wall of the container. So to improve the control a foam has over the motion of non-spherical objects, we would need to consider more complicated ordered foams such as the staircase, twisted staircase or double staircase foams [15].

Future work may include an investigation of how the interaction between a soap film and a solid object varies for other shapes such as ellipsoids, as well as the surface properties of the object and the wetting film covering it. For the latter, the contact angle between the soap film and the descending object would need to be varied, introducing the possibility of including frictional forces into our model. It would also be interesting to investigate how the interaction between foams and solid objects varies with the choice of ordered or disordered foams, of different foam wetness and polydispersity.

Data Access

A full set of raw data and source code for a simulation file is included in the electronic supplementary material that is available from Aberystwyth University's open access repository at https://doi.org/10.20391/d47a5e1b-583f-4261-ae87-46d1ce021075 [34].

Acknowledments

Funding from the Coleg Cymraeg Cenedlaethol and the MATRIXASSAY H2020-MSCA-RISE-2014 grant (project number 644175) is gratefully acknowledged. I thank S. Cox for stimulating discussions and K. Brakke for providing and supporting the Surface Evolver.

---

[1] Cantat I, Cohen-Addad S, Elias F, Graner F, Höhler R, Pitois O, Rouyer F, Saint-Jalmes A. 2013 *Foams Structure and Dynamics*. Oxford University Press.

[2] Weaire D, Hutzler S. 2000 *The Physics of Foams*. Oxford University Press.

[3] Rossen WR. 1996 Foams in Enhanced Oil Recovery. In Prud'homme RK, Khan SA, editors, *Foams: Theory, Measurements and Applications*. CRC Press.

[4] Sheng JJ. 2013 Chapter 11 - Foams and Their Applications in Enhancing Oil Recovery. In Sheng JJ, editor, *Enhanced Oil Recovery Field Case Studies* pp. 251 – 280. Boston: Gulf Professional Publishing.

[5] Prud'homme RK, Warr GG. 1996 Foams in Mineral Flotation and Separation Processess. In Prud'homme RK, Khan SA, editors, *Foams: Theory, Measurements and Applications*. CRC Press.

[6] Shean B, Cilliers J. 2011 A review of froth flotation control. *International Journal of Mineral Processing* **100**, 57 – 71.

[7] Feng Dx, Nguyen AV. 2017 Effect of contact angle and contact angle hysteresis on the floatability of spheres at the air-water interface. *Advances in colloid and interface science* **248**, 69–84.

[8] Xing Y, Gui X, Pan L, Pinchasik BE, Cao Y, Liu J, Kappl M, Butt HJ. 2017 Recent experimental advances for understanding bubble-particle attachment in flotation. *Advances in colloid and interface science* **246**, 105–132.

[9] Schellenberger F, Papadopoulos P, Kappl M, Weber SA, Vollmer D, Butt HJ. 2018 Detaching microparticles from a liquid surface. *Physical Review Letters* **121**, 048002.

[10] Drenckhan W, Cox S, Delaney G, Holste H, Weaire D, Kern N. 2005 Rheology of ordered foams – on the way to Discrete Microfluidics. *Colloids and Surfaces A: Physicochemical and Engineering Aspects* **263**, 52 – 64.

[11] Raven JP, Marmottant P, Graner F. 2006 Dry microfoams: formation and flow in a confined channel. *Eur. Phys. J. B* **51**, 137–143.

[12] Marmottant P, Raven JP. 2009 Microfluidics with foams. *Soft Matter* **5**, 3385–3388.

[13] Huerre A, Miralles V, Jullien MC. 2014 Bubbles and foams in microfluidics. *Soft Matter* **10**, 6888–6902.

[14] Whitesides GM. 2006 The origins and the future of microfluidics. *Nature* **442**, 368–373.

[15] Davies IT, Cox SJ. 2012 Sphere motion in ordered three-dimensional foams. *J. Rheol.* **56**, 473–483.

[16] Brakke K. 1992 The Surface Evolver. *Exp. Math.* **1**, 141–152.

[17] Courbin L, Stone H. 2006 Impact, puncturing, and the self-healing of soap films. *Physics of Fluids* **18**, 91105–91105.

[18] Goff AL, Courbin L, Stone HA, Quéré D. 2008 Energy absorption in a bamboo foam. *EPL* **84**, 36001.

[19] Cantat I, Pitois O. 2005 Mechanical probing of liquid foam ageing. *J Phys. Condens. Mat.* **17**, S3455–S3461.

[20] Cantat I, Pitois O. 2006 Stokes experiment in a liquid foam. *Phys. Fluids* **18**, 083302.

[21] de Bruyn JR. 2004 Transient and steady-state drag in a foam. *Rheol. Acta.* **44**, 150–159.

[22] de Bruyn JR. 2005 Age dependence of the drag force in an aqueous foam. *Rheol. Acta* **45**, 801–811.

[23] Raufaste C, Dollet B, Cox S, Jiang Y, Graner F. 2007 Yield drag in a two-dimensional foam flow around a circular obstacle: Effect of liquid fraction. *Euro. Phys. J. E.* **23**, 217–228.

[24] Dollet B, Durth M, Graner F. 2006 Flow of foam past an elliptical obstacle. *Phys. Rev. E* **73**, 061404.

[25] Davies I, Cox S. 2010 Sedimentation of an elliptical object in a two-dimensional foam. *J. Non-Newton Fluid* **165**, 793–799.

[26] Boulogne F, Cox. SJ. 2011 Elastoplastic flow of a foam around an obstacle. *Phys. Rev. E* **83**, 041404.

[27] Morris G, Neethling S, Cilliers J. 2010 The effects of hydrophobicity and orientation of cubic particles on the stability of thin films. *Miner. Eng.* **23**, 979 – 984.

[28] Morris G, Neethling S, Cilliers J. 2011a A model for investigating the behaviour of non-spherical particles at interfaces. *J. Colloid Interf. Sci.* **354**, 380 – 385.

[29] Morris G, Neethling S, Cilliers J. 2011b Modelling the self orientation of particles in a film. *Miner. Eng.* **33**, 87–92.

[30] Dasgupta S, Auth T, Gompper G. 2017 Nano-and Microparticles at Fluid and Biological Interfaces.. *Journal of Physics: Condensed Matter*.

[31] Jaklic A, Leonardis A, Solina F. 2000 Superquadrics and Their Geometric Properties. In *Segmentation and Recovery of Superquadrics*, vol. 20, pp. 13–39. Springer Science and Business Media.

[32] Zhou L, Kambhamettu C. 2001 Extending Superquadrics with Exponent Functions: Modeling and Reconstruction. *Graphical Models* **63**, 1 – 20.

[33] Soligno G, Dijkstra M, van Roij R. 2016 Self-Assembly of Cubes into 2D Hexagonal and Honeycomb Lattices by Hexapolar Capillary Interactions. *Phys. Rev. Lett.* **116**, 258001.

[34] Davies I.T. 2018 Data from Simulating the interaction between a falling super-quadric solid object and a soap film. Aberystwyth University's Open Access Repository (https://doi.org/10.20391/d47a5e1b-583f-4261-ae87-46d1ce021075)